

Article

Enhancing Savonius Vertical Axis Wind Turbine Performance: A Comprehensive Approach with Numerical Analysis and Experimental Investigations

Kumail Abdulkareem Hadi Al-Gburi ¹, Firas Basim Ismail Alnaimi ^{2,*},
Balasem Abdulameer Jabbar Al-quraishi ³, Ee Sann Tan ¹ and Ali Kamil Kareem ⁴

¹ Department of Mechanical Engineering, Universiti Tenaga Nasional (UNITEN), Kajang 43000, Malaysia

² Power Generation Unit, Institute of Power Engineering (IPE), Universiti Tenaga Nasional (UNITEN), Kajang 43000, Malaysia

³ Engineering Technical College of Najaf, Al-Furat Al-Awsat Technical University, Najaf 31001, Iraq

⁴ Biomedical Engineering Department, Al-Mustaqbal University, Hillah 51001, Iraq

* Correspondence: firas@uniten.edu.my

Abstract: Small-scale vertical-axis wind power generation technologies such as Savonius wind turbines are gaining popularity in suburban and urban settings. Although vertical-axis wind turbines (VAWTs) may not be as efficient as their horizontal-axis counterparts, they often present better opportunities for integration within building structures. The main issue stems from the suboptimal aerodynamic design of Savonius turbine blades, resulting in lower efficiency and power output. To address this, modern turbine designs focus on optimizing various geometric aspects of the turbine to improve aerodynamic performance, efficiency, and overall effectiveness. This study developed a unique optimization method, incorporating a new blade geometry with guide gap flow for Savonius wind turbine blade design. The aerodynamic characteristics of the Savonius wind turbine blade were extensively analyzed using 3D ANSYS CFX software. The optimization process emphasized the power coefficient as the objective function while considering blade profiles, overlap ratio, and blade number as crucial design parameters. This objective was accomplished using the design of experiments (DOE) method with the Minitab statistical software. The research findings revealed that the novel turbine design “OR0.109BS2BN2” outperformed the reference turbine with a 22.8% higher power coefficient. Furthermore, the results indicated a trade-off between the flow (swirling flow) through the gap guide flow and the impact blockage ratio, which resulted from the reduced channel width caused by the extended blade tip length.

Keywords: Savonius wind turbine; blade optimization; CFX; design of experiments (DOE); power coefficient; wind tunnel



Citation: Al-Gburi, K.A.H.; Alnaimi, F.B.I.; Al-quraishi, B.A.J.; Tan, E.S.; Kareem, A.K. Enhancing Savonius Vertical Axis Wind Turbine Performance: A Comprehensive Approach with Numerical Analysis and Experimental Investigations. *Energies* **2023**, *16*, 4204. <https://doi.org/10.3390/en16104204>

Academic Editors: Martin Otto
Laver Hansen and Galih Bangga

Received: 17 April 2023

Revised: 9 May 2023

Accepted: 16 May 2023

Published: 19 May 2023



Copyright: © 2023 by the authors. Licensee MDPI, Basel, Switzerland. This article is an open access article distributed under the terms and conditions of the Creative Commons Attribution (CC BY) license (<https://creativecommons.org/licenses/by/4.0/>).

1. Introduction

Wind turbines, classified into two main types, horizontal-axis and vertical-axis turbines, convert the wind’s kinetic energy into electrical power. Vertical-axis wind turbines (VAWTs) generally exhibit lower efficiency than horizontal-axis wind turbines (HAWTs). The primary reason for this difference in efficiency is that the sliding surface of VAWTs provides an effective driving force for only slightly more than half of its total area. During the rotational cycle, the varying angle of attack for VAWTs results in flow detachment, dynamic stalling, and unequal force distribution on both sides of the rotor. Consequently, aerodynamic performance becomes unstable, resulting in oscillation and noise [1–3]. On the other hand, VAWTs possess inherent advantages over HAWTs, such as user-friendliness, lower cost, simpler design, and no need for a yaw system. Savonius rotors belong to a category of vertical-axis wind turbines. The driving torque is generated when the wind’s drag on the blades combines with the cup-shaped blades, which provide a large surface

area for the wind to exert pressure on. Savonius turbines rely on drag force, which is more significant than lift force at low speeds. Due to this, the cup shape partially retains air as the blade rotates, enabling the turbine to operate more efficiently. Furthermore, Savonius turbines are particularly beneficial in remote areas due to their lower initial investment, ongoing costs, and reduced maintenance requirements. Unlike large-scale wind turbines, Savonius rotors have fewer location constraints, making them more versatile for various installation sites [4–6]. The Savonius wind rotor features two semi-cylindrical shaped cylinders. In principle, the pressure disparity between the two turbine blades generates rotational motion. The Savonius rotor presents various benefits, such as a substantial self-starting torque and the capacity to function independently of the wind's direction. However, compared to other wind turbine types, their efficiency is generally lower.

Several review articles [7–10] provide comprehensive discussions on experimental and numerical research outcomes for wind turbines. The impact of geometric factors on the aerodynamic performance of turbines has captured the attention of many researchers. By modifying parameters such as aspect ratio (AR), overlap ratio (OR), twist angle (TA), and blade number (BN), significant performance improvements have been observed in numerous studies. Moreover, significant discoveries have been made in Savonius's wind turbine design [11]. The efficiency of Savonius wind turbines can be enhanced by incorporating an overlap area between the blades, which allows the wind to circulate back into the returning blade and generate positive torque [12]. The effectiveness of this approach has been demonstrated by comparing the power generation of turbines with and without the overlap section [13]. Ebrahimpour et al. [14] found that optimal performance for a turbine could be achieved with an OR between 0.10 and 0.15, which is consistent with experimental results. This conclusion was drawn by comparing the performance of blades with equal overlaps along the X and Y axes. Furthermore, numerical simulations [15] have indicated that the elliptical profile significantly improves performance at an OR value of 0.15. In their research, R. Hassanzadeh and M. Mohammadnejdd investigated various overlap ratios, including 0.1, 0.02, and 0.3. They discovered that the optimal power coefficient value occurs at an inward overlap ratio of 0.2. The optimal power coefficient value also changes as the overlap ratio varies in either direction [16]. Researchers analysed the rotor blades' pressure distribution to comprehend better the critical low-pressure and high-pressure areas that contribute to the overall torque output of Savonius turbines [17]. Experimental findings indicate that adjusting the geometry of blades in a Savonius rotor wind turbine can lead to an enhanced power coefficient. These results highlight the possibility of optimizing the turbine's performance by strategically modifying blade geometry [18,19]. An alternative optimization approach is the design of experiments (DOE), which primarily aims to select specific design parameters that effectively represent the design space. Given the relatively small number of control points, employing a factorial method is an appropriate strategy [20]. By using DOE , researchers can systematically explore the relationships between design factors and outcomes, enabling a more comprehensive understanding of the design space and facilitating the identification of optimal solutions [21]. Blades with a regular zigzag pattern on their inner surfaces were tested in an open wind tunnel. A 2D Mode simulation at an overlap ratio of 0.2 yielded the highest power coefficient, which was 3.04% higher than at a 0.15 overlap ratio and 5.54% higher than at a 0.1 overlap ratio [22]. However, the number of blades is another important geometric factor influencing wind turbine performance [23–25]. Researchers compared a two-blade Savonius wind turbine and a three-blade Savonius wind turbine with identical blade types to demonstrate this effect [26].

This research conducts an in-depth numerical analysis of novel blade geometry and guide gap flow, focusing on turbulence effects that influence Savonius wind turbine performance. By understanding and incorporating these effects into rotor blade profile design, improvements in aerodynamic performance and efficiency are achieved. Computational simulations are fine-tuned using a statistical method and full factorial experimental design (FFD) for evaluating parameters, including the power coefficient (C_p) assessment. To confirm the accuracy of the numerical outcomes, they are compared with the most recent

experimental data, which ultimately helps enhance the efficiency of Savonius wind energy conversion systems.

2. Specification of the Numerical Modeling

A comprehensive simulation study using computational fluid dynamics (CFD) software was conducted on a Savonius wind turbine with elliptical blades. The aim was to evaluate the impact of various blade profiles on the total efficiency of the turbine rotor. This in-depth investigation helped to identify the optimal blade profile for improved efficiency and power output. Simulation analysis was conducted on a Savonius wind turbine with elliptical blades to evaluate how blade profiles affect turbine rotor performance. The geometric parameters employed in the computational analysis, including a height-to-diameter ratio (H/D) of 1, an ellipticity (e) of $D/5$ (equivalent to $d/3$, or 0.2), and a blade number (BLN) of 2, were based on the scaled reference model from previous research [27].

Utilizing this scaled reference model enables the recognition of advancements and a more thorough understanding of the effects of various design selections on the turbine's total performance. Figure 1 illustrates the fundamental aspects of the utilized geometry, including its dimensions and features. Additionally, the reference model is a benchmark for validating computational and experimental results, ensuring that the study's findings are consistent with existing research.

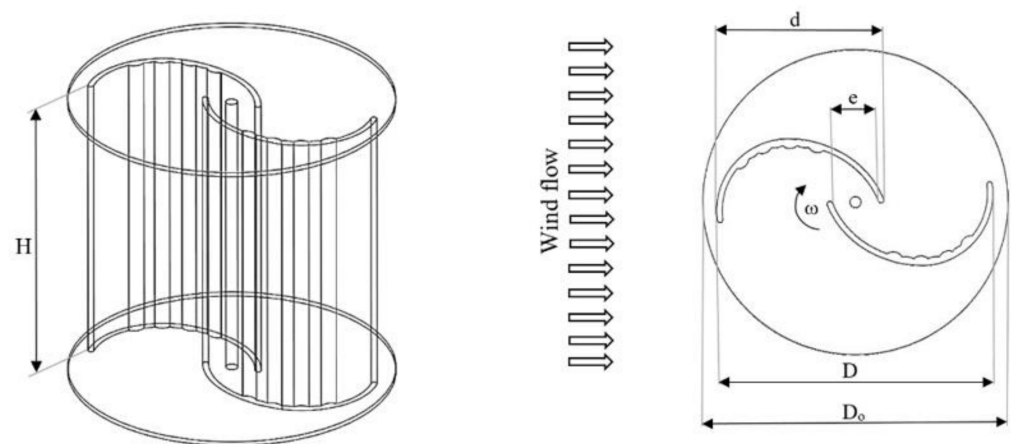


Figure 1. Turbine Design Parameters: ' H ' (rotor height), ' D ' (rotor diameter), ' d ' (blade chord length), ' e ' (overlap distance), ' Do ' (end plate diameter), and ' ω ' (angular velocity).

Initially, the aspect ratio (AR) was identified as the difference between the turbine's height (H) and diameter (D), as depicted in Equation (1). Furthermore, elements (e) and (d) were linked using the overlap ratio (OR) operator, as demonstrated in Equation (2). Additionally, the turbine rotor's frontal swept area (A) was utilized to assess the model's performance, as outlined in Equation (3).

$$AR = \frac{H}{D}, \quad (1)$$

$$OR = \frac{e}{d}, \quad (2)$$

$$A = HD. \quad (3)$$

Figure 1 illustrates the standard Savonius model rotor, employed as the reference model (RM), with parameter definitions including a top (Do) of 165 mm and a maximum (H) of 150 mm. Consequently, the rotor's (D) was equal to 150 mm. The rotor blade thickness was 3 mm, assuming an (AR) of 1 (H/D), an (OR) of 0.2, and a total of 2 blades on

the rotor. The blade thickness of 3 mm was selected based on previous studies and practical considerations for manufacturing and structural stability.

3. Numerical Method

In this study, the computational domain geometry was created in two phases using SolidWorks and ANSYS CFX software, as illustrated in Figure 2, showcasing the 3D computation scope. The complexity and time requirements of 3D simulations can be challenging due to their demand for substantial computational resources. Overcoming these challenges may involve investing in more powerful computational resources or employing more efficient simulation techniques that reduce computational time without compromising the accuracy of the results. A series of transient Computational Fluid Dynamics (CFD) simulations were conducted to assess the performance of the rotor for each simulation case. The Reynolds-Averaged Navier–Stokes (RANS) equations were solved using ANSYS CFX 2020R1 software, employing a second-order-accurate finite-volume discretization scheme.

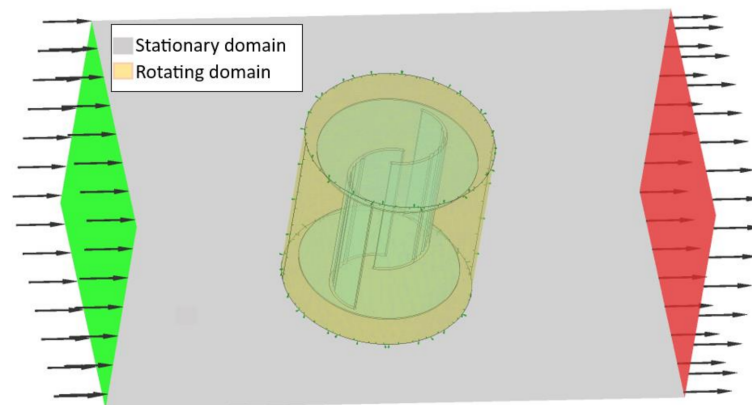


Figure 2. Displays the 3D computational domain, accompanied by the associated boundary conditions.

The governing equations for this study are based on the Reynolds-Averaged Navier–Stokes (RANS) equations, which include the continuity equation and the momentum equation as displayed below [28]:

$$\frac{\partial \rho}{\partial t} + \frac{\partial \rho v'_i}{\partial x_i} = 0, \quad (4)$$

$$\begin{aligned} \frac{\partial}{\partial t}(\rho v'_i) + \frac{\partial}{\partial x_i}(\rho v'_i v'_j) &= -\frac{\partial p}{\partial x_i} + \frac{\partial}{\partial x_i} \left[\mu \left(\frac{\partial v'_i}{\partial x_j} \right) + \left(\frac{\partial v'_j}{\partial x_i} \right) - \frac{2}{3} \delta_{ij} \frac{\partial v'_l}{\partial x_l} \right] \\ &+ \frac{\partial}{\partial x_i}(\rho v'_i v'_j) + F_i \end{aligned} \quad (5)$$

In these equations, ρ represents the fluid density, v_i corresponds to the velocity components, p signifies the total pressure, F_i denotes the external body force components, and μ is the dynamic viscosity. The velocity v_i can be expressed as the sum of the time-averaged value \bar{v}_i and the fluctuating component v'_i .

The Shear Stress Transport (SST) k - ω turbulence model is chosen to model the turbulence terms of the RANS equations [29]. The turbulent kinetic energy (k) and specific dissipation rate (ω) are computed using the following equations:

$$\frac{\partial}{\partial t}(\rho k) + \frac{\partial}{\partial x_i}(\rho k u_i) = \frac{\partial}{\partial x_j} \left[\left(\Gamma_k \frac{\partial \omega}{\partial x_j} \right) + G_k - Y_k + S_k \right], \quad (6)$$

$$\frac{\partial}{\partial t}(\rho \omega) + \frac{\partial}{\partial x_i}(\rho \omega u_i) = \frac{\partial}{\partial x_j} \left[\left(\Gamma_\omega \frac{\partial \omega}{\partial x_j} \right) + G_\omega - Y_\omega + D_\omega + S_\omega \right] \quad (7)$$

In these equations, G_k and G_ω represent the generation of k and ω due to turbulent mean-velocity gradients, respectively; Γ_k and Γ_ω denote the effective diffusivity; Y_k and Y_ω indicate the dissipation of k and ω due to turbulence; D_ω refers to the cross-diffusion term; and S_k and S_ω are user-defined source terms.

The wind tunnel test dimensions were employed to define the computational domain, which included wind flow and rotor rotation domains (test section). The stationary domain was characterized by velocity intake, exit pressure, and a no-slip wall. The rotor domain was 1.1 times the rotor diameter (D), with a 150 mm diameter. The frozen rotor model was essential in establishing a connection between the rotor and stationary domains, enabling the seamless integration of these two distinct regions in the simulation process. This model facilitated the accurate representation of the interaction between the moving rotor and the stationary components. However, during the simulations, the rotor domain rotated at a wind speed of 9 m/s, and an unsteady effect analysis was performed for all cases. The simulation utilized 40-time steps per rotor rotation and six processing cores, taking five hours to complete. A transient rotor-stator (TRS 360) interface model was also developed for 3D viscous flutter research. During the simulation, one to three internal iterations were necessary for each time step. Precise root mean square (RMS) outcomes could be achieved by ensuring the rotor completed four rotations.

This study employs an unstructured mesh topology to demonstrate its flexibility and effectiveness in generating a high-quality mesh for rotating and fixed domains. Unstructured meshes offer a meshing approach that does not rely on predefined patterns or shapes, allowing for efficient mesh generation in complex geometries. As shown in Table 1, a grid independence investigation was conducted to evaluate mesh quality regarding skewness and orthogonality. This analysis ensures that the mesh is refined to an appropriate degree, leading to accurate and reliable results while maintaining computational efficiency. The unstructured mesh approach provides a robust and adaptable solution for handling diverse and intricate geometries, making it a valuable tool for computational fluid dynamics simulations in the context of wind turbine blade design and analysis.

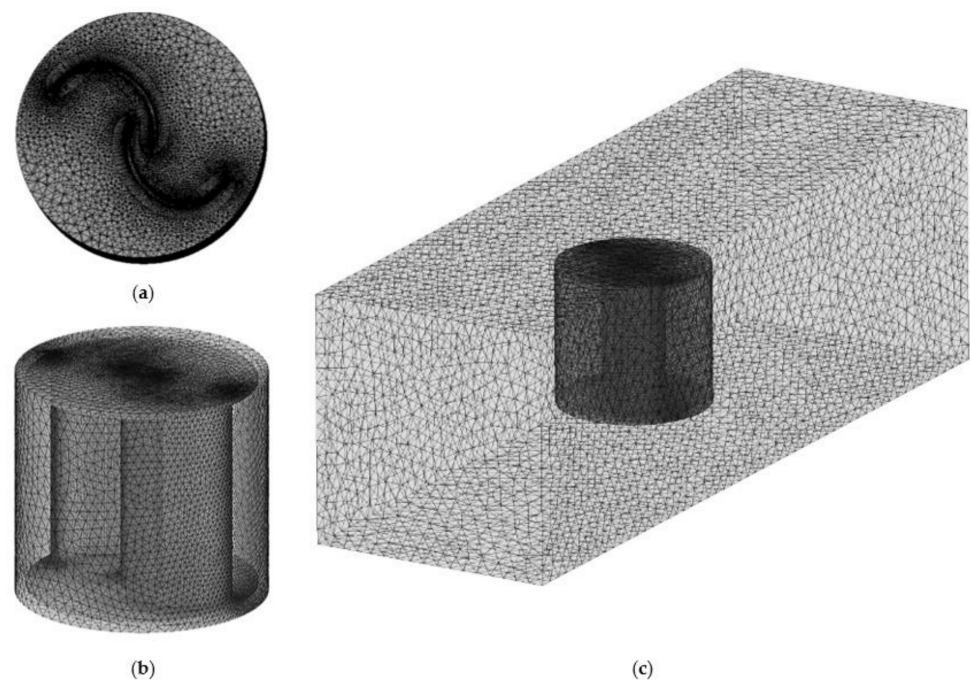
Table 1. Summarizes the mesh, which identifies the stationary and rotating domains.

Grid	Stationary Domain		Rotating Domain	
	No. of Elements	No. of Nodes.	No. of Elements	No. of Nodes.
Coarse	83,352	27,871	1,757,235	925,883
Medium	194,725	37,101	2,129,990	2,746,720
Fine	231,272	327,557	2,488,752	3,729,226
Extra fine	632,023	235,274	4,391,444	5,254,209

In this study, the power coefficient (C_p), a critical parameter for assessing wind turbine performance, was determined using a comprehensive meshing approach. This method produced 4,056,000 elements for both rotating and stationary domains, as detailed in Table 2. A tetrahedral technique was utilized to inflate and refine the mesh surrounding the rotor wall, as depicted in Figure 3. The test simulation commenced with a maximum of five inflation layers at a 1.1 growth rate, according to Table 2. To guarantee a $y^+ < 5$ in all operational conditions, the initial layer thickness perpendicular to the wall was established at 0.000122 m.

Table 2. Justifies the chosen mesh size by presenting statistics on grid independence.

Density of Mesh	Coarse	Medium	Fine	Extra Fine
Total number of elements	1,840,587	2,324,715	2,720,024	5,023,467
Total number of nodes	953,754	2,783,821	4,056,783	5,489,483
Inflation numbering	5	10	15	20
Growth rate inflation	1.1	1.1	1.1	1.1
Skewness average	0.842	0.839	0.811	0.837
Orthogonal quality average	0.989	0.992	0.994	0.993
Blade sizing (mm)	2.5	2	1.5	1
Rotating circle face sizing (mm)	15	10	5	2.5
Outer domain face sizing (mm)	20	15	10	5

**Figure 3.** Mesh setup on (a) turbine blades, (b) revolving domain, and (c) stationary domain.

To further justify the chosen mesh size and type, grid independence statistics were evaluated on DOE models where the same meshing method applied to all the models in the study was adopted, ensuring consistent and accurate results. This approach demonstrates the study's commitment to maintaining the reliability and accuracy of the computational outcomes, providing confidence in the findings obtained from the DOE models. The computational results and verifying were appropriate and robust.

To confirm the accuracy of the simulation results, they were compared to the experimental data gathered at a wind speed of 9 m/s. The C_p values derived from the simulation findings were evaluated against the experimental data for the reference model. The results showed a maximum relative error of 8% for TSRs between 0.2 and 1.8 with an overlap ratio of 0.2 as shown in Figure 4. A minor discrepancy between the model and experimental data was observed at higher tip speed ratios, with the simulation slightly overestimating the values. In contrast, the experimental data tended to underestimate the values at lower TSRs. A more comprehensive understanding of its importance in assessing wind turbine performance is achieved by addressing the significance of C_p early in the research.

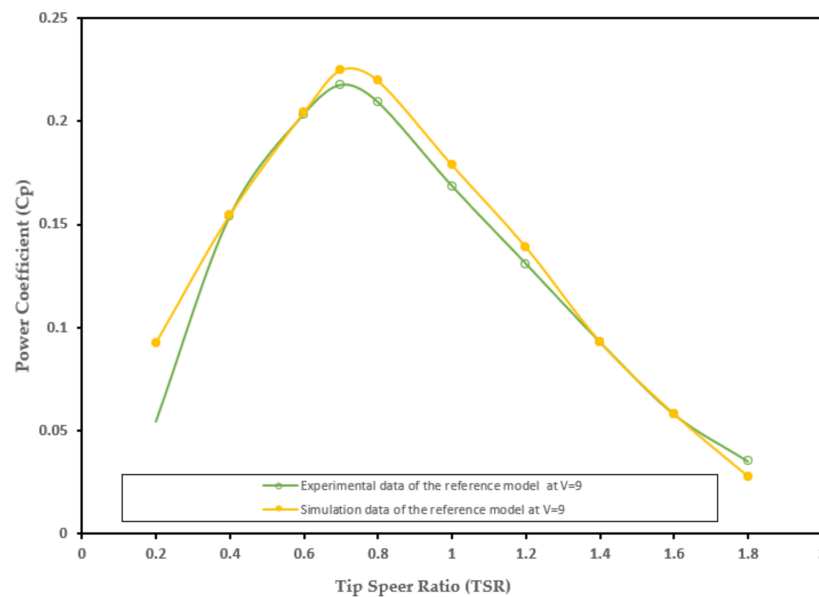


Figure 4. Comparison of C_p values from simulation and experimental data for the reference model.

In transient simulations, the best convergence was achieved when variables approached the specified reference values, with twenty iterations per time step [30]. All simulations utilized absolute convergence for continuity, velocity components, and turbulence, adhering to *CFX*'s residual targets of 10^{-4} . Figure 5 illustrates the instantaneous torque variation of a Savonius turbine against incremental time steps at *TSR* values ranging from 0.2 to 1.8. The highest C_p was observed at *TSR* = 1. Convergence was achieved after two turbine revolutions, with four rotations in total.

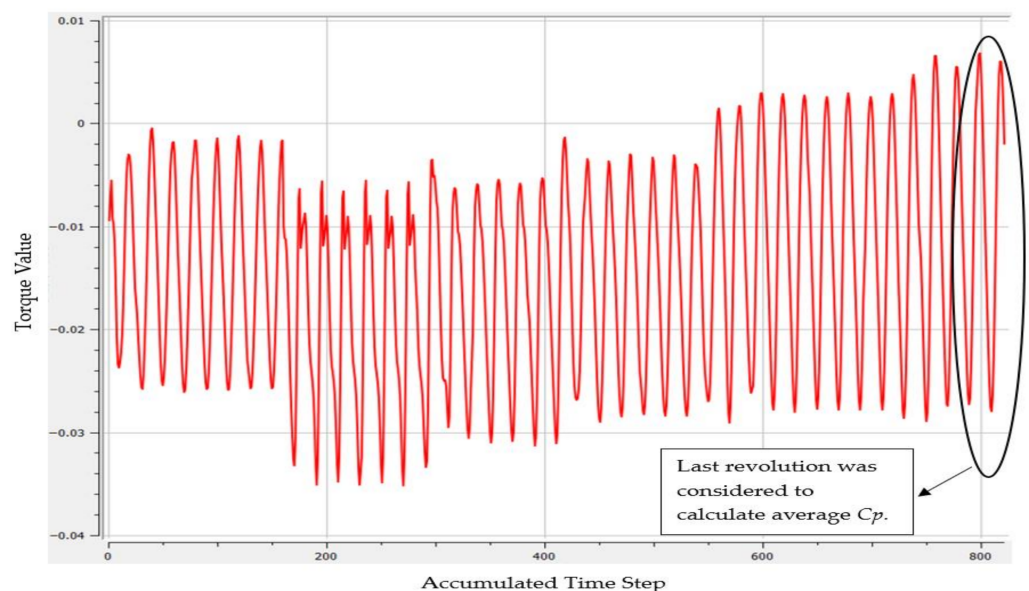


Figure 5. Instantaneous torque variation of a Savonius turbine against cumulative time steps.

Researchers conducted numerical simulations to assess each angular position's rotor axis torque coefficient (C_T). The periodicity was stabilized by averaging the last two complete rotations after a total of four turbine revolutions. Using this average C_T value, C_p was estimated for all geometries with the help of Equation (3). By accurately analyzing the C_p and C_T values, this comprehensive approach represents the turbine's performance under various conditions, thereby contributing to a more in-depth understanding of the underlying factors and their impact on wind turbine efficiency.

The power coefficient (C_p) and tip speed ratio (TSR) express wind energy efficiency. C_p represents the maximum efficiency of a wind turbine to transform air's kinetic energy into rotational energy. Concurrently, TSR denotes the rotor blade's tip speed in proportion to the free-stream wind speed. The power generated by the rotor was calculated by multiplying its torque (T) by its rotational velocity (ω). These equations are crucial for assessing wind turbine performance under various conditions [31]. Another method of characterizing the wind's influence on a rotor involves the torque coefficient (C_T), which is the ratio of the rotor's actual torque (T_w) to the theoretical torque (T) [32]:

$$C_P = \frac{P_{turbine}}{P_{wind}} = \frac{T\omega}{0.5 \rho A V_{\infty}^3}, \quad (8)$$

$$TSR = \frac{\omega R}{V_{\infty}}, \quad (9)$$

$$C_T = \frac{\text{Actual torque}}{\text{Theoretical torque}} = \frac{T_{turbine}}{T_w} = \frac{T}{0.5 \rho A R V_{\infty}^2} = \frac{C_P}{TSR}. \quad (10)$$

where ρ is air density (mass per unit volume) at the location of the wind turbine, which at 30 degrees Celsius is 1.165 kg/m^3 , T is the torque in Newton-meters generated by the rotor, influenced by the wind acting on the turbine blades, T_w is the theoretical torque, A is the swept area of the turbine rotor, which is the area covered by the rotation of the blades, R is the effective radius of the turbine in meters, V_{∞} is the free-stream wind velocity (wind speed) upstream of the turbine, and ω is the angular velocity (rotational speed) of the rotor in radians per second. The torque produced in the experiment was calculated as follow in according to [33].

$$T_{turbine} = F r = 9.81 (W - S)(rp + dr). \quad (11)$$

where F and r are the pulley's load and radius, respectively. W represents the side tight tension in kilograms, S the side slack in kilograms, rp the pulley radius in meters, and dr the nylon string diameter in millimeters (m).

4. Optimization Process

The suggested design process consists of three primary phases. The initial phase entails the creation of a numerical model and the definition of the new blade profile. In the second phase, an optimization procedure is carried out to attain the best aerodynamic performance, using the Design of Experiments (*DOE*) approach. Finally, the optimal model is identified through experimental evaluations. Figure 6 depicts a flowchart demonstrating the design methodology's sequence and connections.

4.1. Choosing Geometric Parameters for Savonius Wind Turbines

Different design parameters, including blade profile, overlap ratio, and blade number, influence the aerodynamic performance of a wind turbine. The blade profile under examination is derived from an ellipse with a semi-minor to semi-major axes ratio of $2/3$. The optimal result for the C_T and C_p is achieved by sectioning the ellipse at an angle ($\theta = 47.5^\circ$). Specific blade profile configuration has been developed to impact the wind turbine's overall performance significantly (please refer to Section 4.2). The selection of geometric parameters for the Savonius turbine was informed by an extensive literature review and a systematic approach that investigated (please refer to Section 4.3) the impact of various factors on the response variable. The evaluation was carried out using *ANSYS CFX* software and different blade profiles. The fluctuations in power coefficients were observed, leading to an optimal blade profile selection.

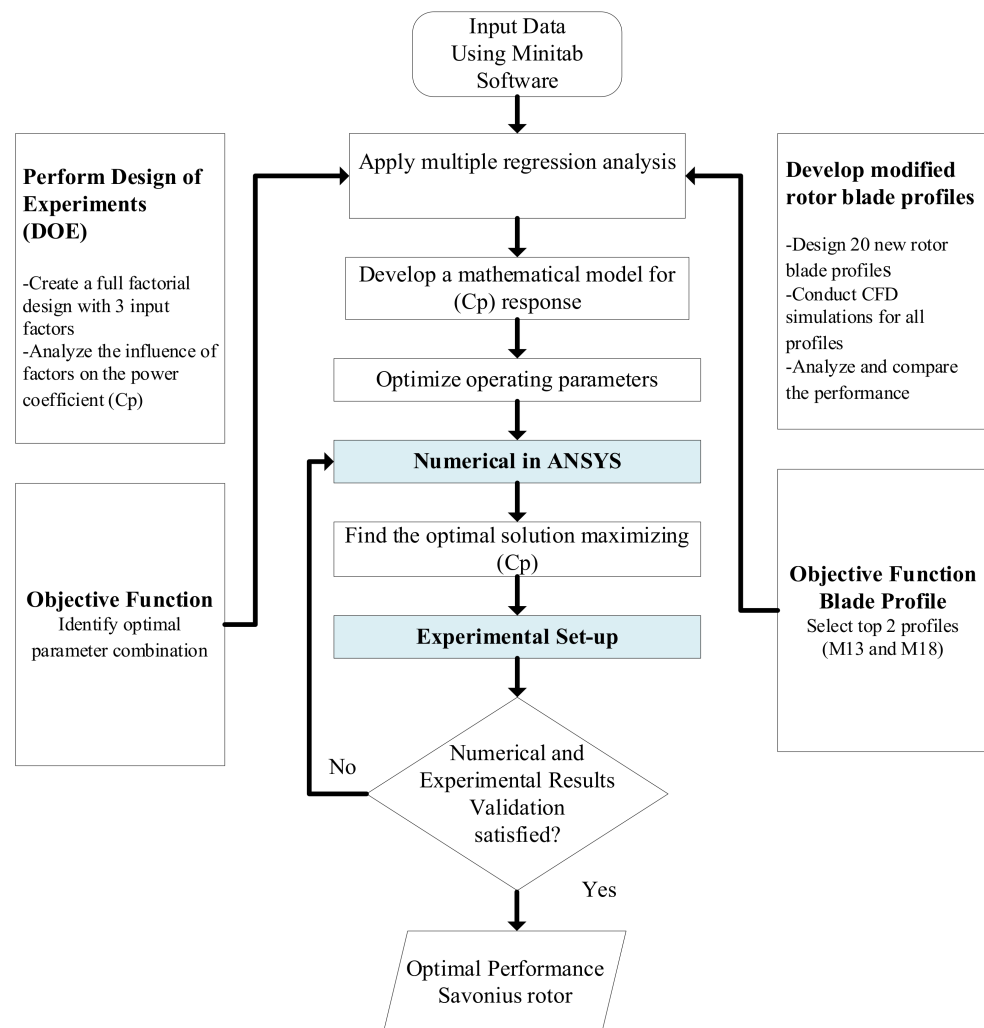


Figure 6. Flowchart illustrating the optimization process.

4.2. Determination of the Optimum Blade Shape Inner Profile

The selection of an appropriate blade shape is essential in achieving the intended performance of a Savonius wind turbine. This section presents a detailed examination of various profiles for the inner blade shape. The primary objective was to analyze each inner blade shape profile, pinpoint the most appropriate regions for the inner profile, and incorporate a gap flow guide.

In Figure 7, ten distinct inner blade profiles designated *M1* to *M5* and *M11* to *M15* were carefully positioned at the blade arc's center to investigate their influence on the blade's performance. *ANSYS CFX* was employed to analyze and compare their performance based on the wavy area distributions and corresponding C_p values under optimal conditions for each profile. Subsequently, ten gap guide flows (*M6* to *M10* and *M16* to *M20*) were incorporated into the design to improve blade geometry. These gap guide flows were introduced to better manage airflow and evaluate their impact on the overall performance of the wind turbine. By combining the inner wavy area profiles and gap guide flows, this comprehensive analysis of various blade geometries allows for the identification of the most effective design to enhance aerodynamic performance.

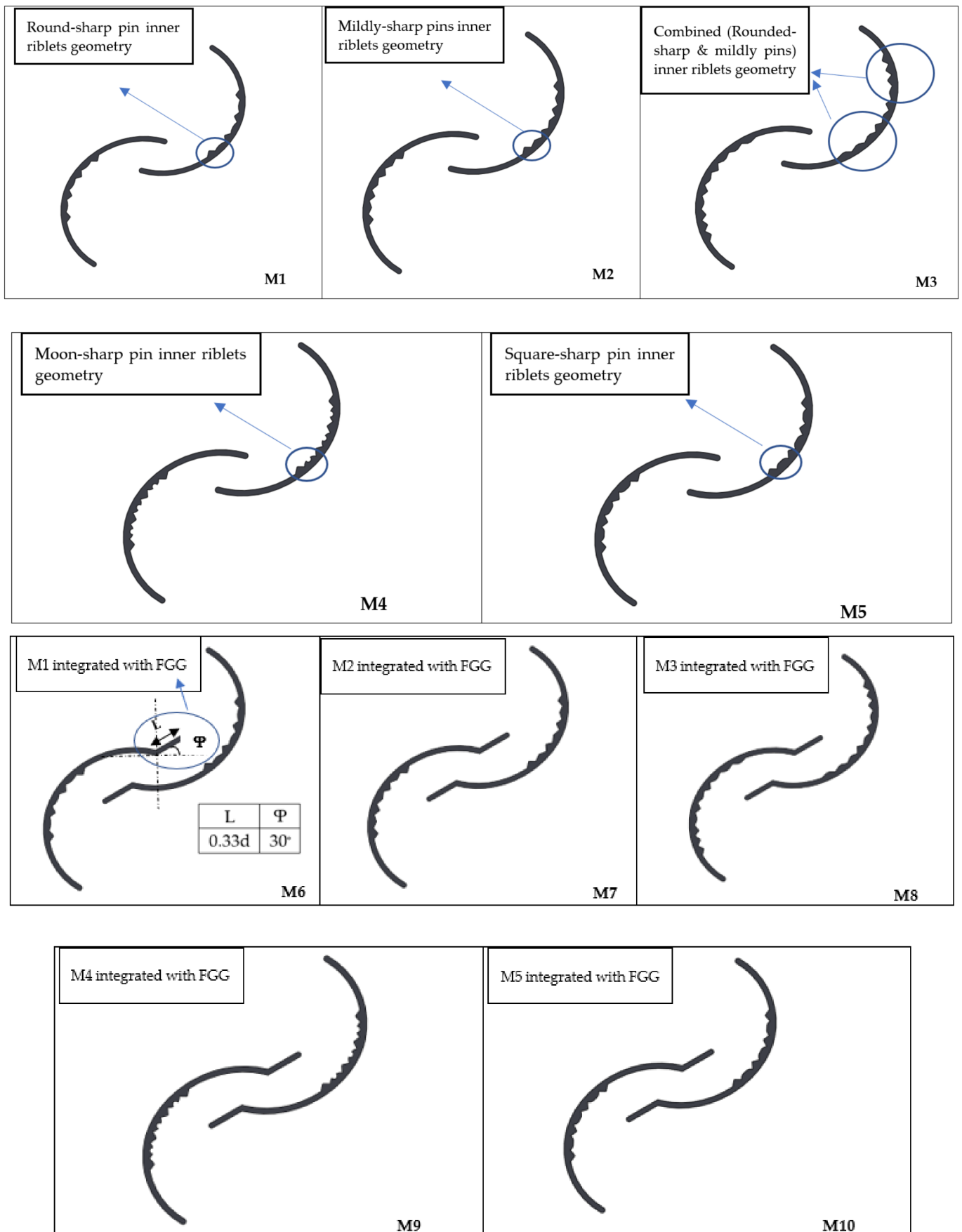


Figure 7. Cont.

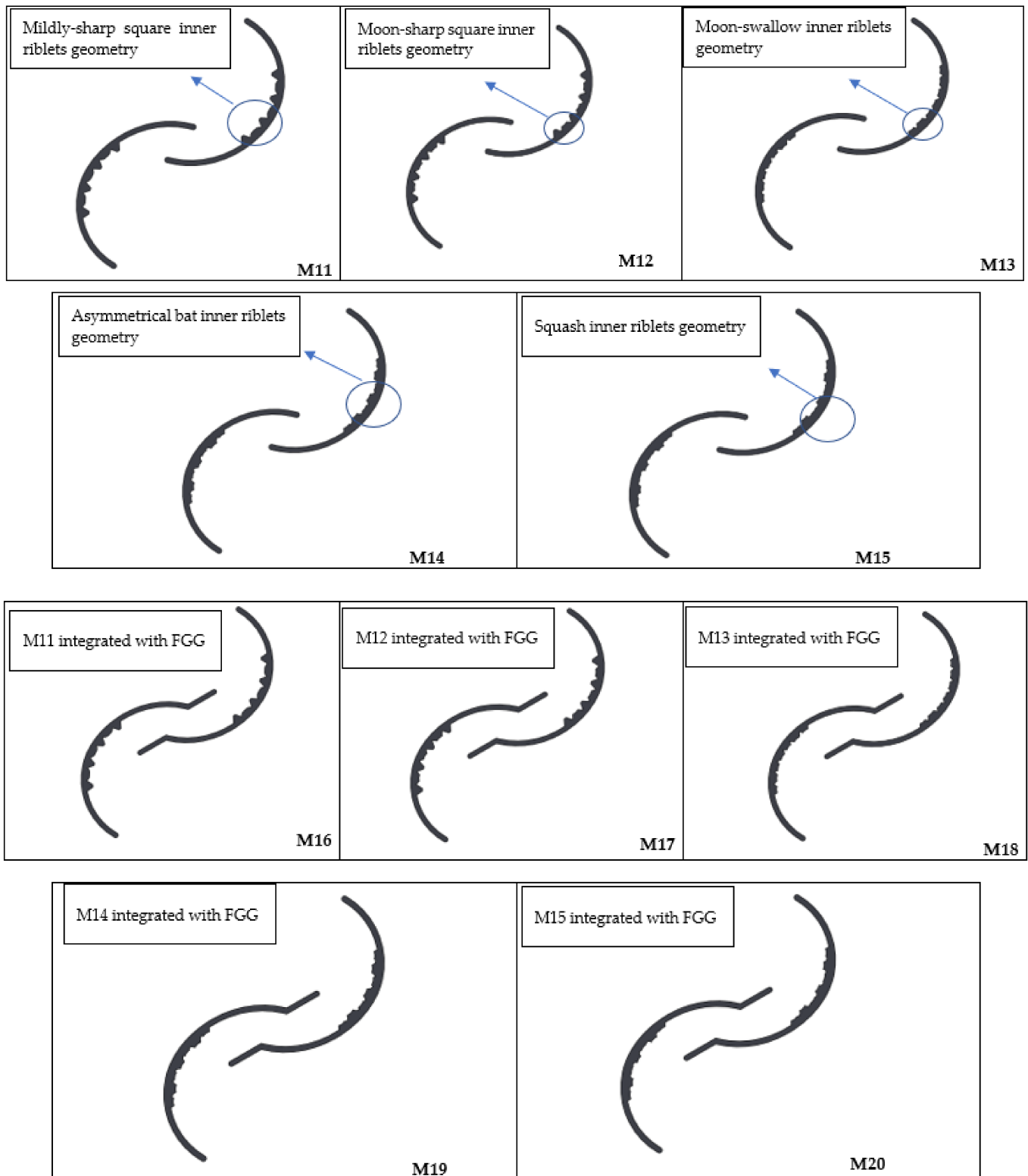


Figure 7. Illustrating the area blade profile configurations.

4.3. Evaluating Parameters with Design of Experiments (DOE) Method

DOE is a statistical methodology to determine and analyze significant factors in a given process. A factorial approach, represented by 2^n , was utilized to examine each factor thoroughly. Minitab 17 software facilitated the design of a full factorial experiment incorporating three input factors: overlap ratio, blade shape, and the number of blades. As demonstrated in Table 3, each of these factors has two levels.

Table 3. Factors and Levels for the Current Investigation.

Factors	Min Level	Max Level
Blade Shape	1 (M13)	2 (M18)
Overlap ratio	0.1	0.2
Blade Number	2	3

The Design of Experiments (DOE) assessed eight distinct blade configurations, which considered three independent variables. This resulted in a total of eight simulation runs, as detailed in Table 4. The *Minitab* software was employed to optimize the simulation outcomes within specified domains. By conducting these 8 runs, a systematic evaluation of the different blade designs was achieved, ultimately leading to the identification of the optimal configuration to maximize wind turbine performance.

Table 4. Summary of the Eight Blade Configurations Examined Based on Three Independent Variables in the DOE.

Experiment No.	Overlap Ratio (OR)	Blade Shape (BS)	Blade Number (BN)	C_p
1	0.2	1	3	0.25741
2	0.2	2	2	0.26186
3	0.1	2	3	0.23911
4	0.1	2	2	0.27001
5	0.1	1	2	0.25966
6	0.2	1	2	0.24955
7	0.1	1	3	0.23724
8	0.2	2	3	0.25866

To determine the impact of the regression model's terms on the response variable C_p , R^2 and p -value statistics were assessed. The suitability of the generated equation was further evaluated, and the optimal solution was identified as the combination that maximizes C_p . However, it is essential to note that while CFD studies can accurately assess the influence of the involved variables, they may sometimes exaggerate or minimize the effects of these components compared to previous findings. Therefore, experimental testing was conducted to validate the optimization results and ensure their accuracy, providing a more reliable basis for the conclusions drawn from the study.

5. Experimental Setup

The experiments were conducted to evaluate the simulations' accuracy and offer a basis for comparing different blade configurations. This approach helps to validate the findings obtained from the simulations and ensures a comprehensive understanding of the performance of each design under real-world conditions. Figure 8 presents a subsonic open-type wind tunnel used for testing at Al-Furat Al-Awsat Technical University (ATU) aerodynamic lab in Iraq. The experiment involved varying the wind blowing rate from 1 to 32 m/s. It is important to note that the size of the wind tunnel test section was 600 mm in length, 305 mm in width, and 305 mm in height. Despite the seemingly small dimensions of the test section in comparison to the turbine size, the blockage percentage in this study was determined to be acceptable, as per the investigation mentioned in reference [27]. Consequently, no blockage correction measures were used or applied in

this research, ensuring that the experimental results accurately represented the turbine's performance under various wind conditions. The dynamic torque was obtained using a rope brake dynamometer that employed a belt rope tied to the spring that could be applied by tightening nuts [34]. A digital laser tachometer DT-2268 was used.

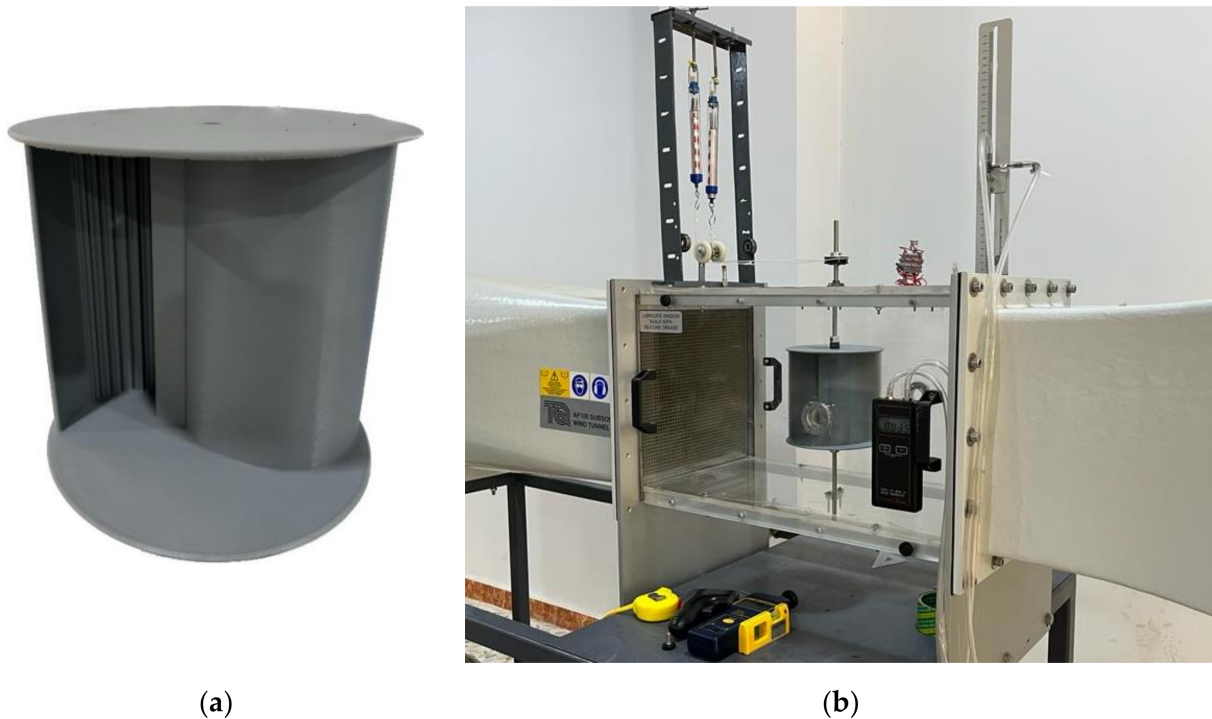


Figure 8. Optimized Savonius wind turbine: (a) printed model and (b) installation model in test section.

The turbine model started unloaded. Increasing the pulley's braking belt tension slowed the rotating turbine model. Hence, the tip speed ratio (TSR), rotor torque (T), torque coefficient (C_T), and power coefficient (C_p) were calculated by measuring the forces applied during braking using spring weight at different revolutions per minute (RPM) values. Each following increment was increased by 1 g until the shaft stopped rotating. Experiments were carried out for each configuration to capture data. C_p and C_T were compared for the new optimized model turbine's power output. The wind velocity was tested for accuracy and uncertainty using a digital manometer 475 and compared with a Pitot static tube [35]. Finally, the measurement is taken under consistent and representative conditions. Wind speed, direction, and turbulence can all affect the rotor's performance and the measurement's accuracy. The limitations in the experiment stem from the inherent uncertainties in the measurements, which can affect the accuracy of the results. Such uncertainties arise from the inability to determine the true value and the reliance on calibration with more accurate instruments to approximate it. These measurement limitations can impact the calculated outcomes, making it essential to account for potential deviations in the experimental process. Multiple measurements were taken under different conditions to address this issue, and the results were averaged to obtain a more accurate measure of the power output. In each realistic replication of the experiment, the total uncertainty of the model was assessed, and the uncertainties were found to be closely matched and acceptable. This approach helps mitigate the effects of measurement limitations on the study's outcomes.

6. Results and Discussion

6.1. Determination of the Optimum Blade Shape Inner Profile

Using *ANSYS CFX*, the modified rotor inner profiles were modelled to evaluate the actual turbine performance better. The optimization process focuses on the highest achievable C_p at a TSR of 1 to simplify the analysis. This approach enables researchers to concentrate on the immediate effects of varying blade profiles on turbine performance, thereby facilitating the identification of the most effective profile for the specified TSR . Figure 8 compares the maximum power generation in the reference model (*RM*) and the modified model for each profile. Additionally, the enhanced performance of the modified inner blade profiles compared to the reference model is evident, signifying that the various profile configurations contributed to the overall improvement in performance. Models *M13* and *M18* displayed the most exceptional performance among the optimized inner blade profiles. Analyzing the C_p values obtained for different configurations, it is evident that models 13 and 18 had notably higher C_p values than the others. Figure 9 displays the variations in the numerical analysis results for the twenty selected blade profiles chosen to cover a comprehensive range of design possibilities. The relatively small difference in C_p for several designs in Figure 9 can be attributed to the presence of a gap guide flow integrated into the profiles. The development of flow near the entrance causes substantial turbulence, which impacts the overall performance of the various designs, resulting in less significant C_p differences among the selected blades profiles.

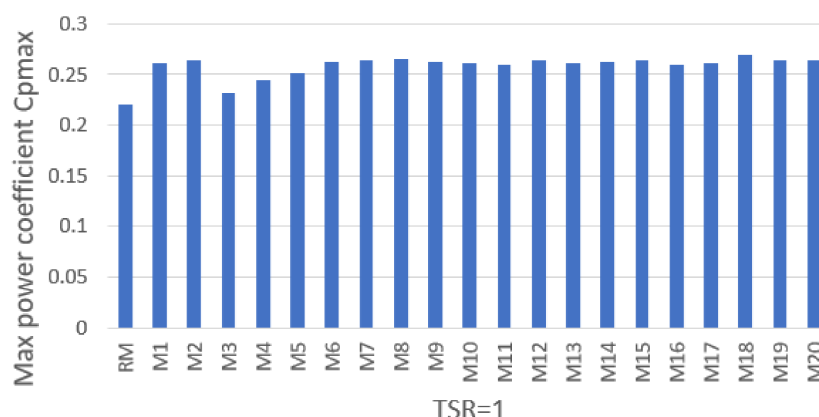


Figure 9. Max performance of various blade configurations related to the reference model.

6.2. Effects of Chosen Parameters on Overall Performance

The testing of the performance of an updated configuration of the Savonius rotor to evaluate the degree to which it has been improved was the second aim of this body of work.

Upon obtaining the optimal two-blade profiles (*M13* and *M18*), as depicted in Figure 6, these two profiles were investigated for level selection to identify the optimal parameters for further analysis. The full factorial design (*FFD*) was employed to ascertain the significant influence of each control factor's level on the target response. Consequently, the level with the most substantial impact was selected to enhance the C_p value. The optimization procedure occurred at a Tip Speed Ratio (TSR) of 1, selected to keep the rotor speed steady and manageable, thus streamlining the analysis. The data was evaluated using the *Minitab 17.0* software tool to determine the optimal design parameters. Table 4 displays the outcomes of 8 iterations of each combination performed with *ANSYS CFX*. The power coefficients are plotted against the values of three independent variables, the overlap ratio, the form of the blades, and the number of blades. Between eight experiments, the optimum configuration was found as *OR0.1BS2BN2*. After identifying the optimal configuration, *OR0.1BS2BN2*, further analysis was conducted to understand the underlying reasons for its superior performance compared to other configurations. This step involved examining the interactions between the independent variables and their effects on the power coefficient. It

aimed to gain insights into the design characteristics contributing to improved aerodynamic performance and efficiency.

6.3. Evaluation of Optimal Design Parameters with ANOVA

An analysis of variance (ANOVA) can be performed to evaluate if a significant connection exists between the control factor and the v response. The current ANOVA results are grounded on a general linear model that includes a coefficient of determination employed to assess the model's capacity to explain the observed data. Table 5 displays the findings. After fitting a second-order multiple regression model with interactions, the R^2 value is 99.95%, R^2 (predicted) is 96.64%, and R^2 (adjusted) is 99.63%. These values suggest a robust relationship between the dependent variable (C_p response) and the independent variables (control factors). The statistics highlight the significance of each parameter and their combined impact on the C_p response, with a 5% risk. The p -value denotes the probability of achieving these outcomes with a 95% confidence level and should be less than 0.05 to be deemed significant, according to [36].

Table 5. Regression data summary using ANOVA.

Source	F Value	p Value	T Value	Coefficient
Model	317.71	0.043	1032.54	0.254264
Overlap ratio	112.02	0.060	10.58	0.002606
Blade shape	179.45	0.047	13.40	0.003299
Blade number	625.51	0.025	−25.01	−0.006159
Overlap ratio x Blade shape	0.14	0.774	0.37	0.000091
Overlap ratio x Blade number	884.53	0.021	29.74	0.007324
Blade shape x Blade number	104.62	0.062	−10.23	−0.002519

The relationship between the wind turbine's performance metrics and its independent operational variables was examined by employing multiple regression analysis [37]. Equation (12) presents a mathematical model representing the desired response regarding the modelled variables. The accuracy of the derived equation is assessed by analyzing its R^2 and adjusted R^2 values, which indicate the goodness of fit for the predicted relationship. The regression equation was developed to estimate the C_p value of a Savonius rotor, and Equation (12) demonstrates how the response surface regression analysis can be used to obtain the finalized practical model based on coded coefficients.

$$C_p = 0.34084 - 0.6857 OR + 0.03124 BS - 0.04115 BN + 0.00365 OR \times BS + 0.29295 OR \times BN - 0.010075 BS \times BN \quad (12)$$

Equation (8) represents the regression model that captures the relationship between the power coefficient (C_p) and the predictor variables, which include overlap ratio (OR), blade shape (BS), and blade number (BN). During the optimization process, the code is designed to search for the maximum C_p value by plugging in the domain values of the predictor variables. After analyzing the combinations, the optimal parametric values are identified as $OR = 0.109$, $BS = 2$, and $BN = 2$. These optimal values represent the $OR0.109BS2BN2$ design, which results from optimization. By substituting these values into Equation (8), the predicted power coefficient (C_p) is calculated to be 0.2706. This C_p value indicates that the $OR0.109BS2BN2$ design maximizes the power coefficient per the developed regression model.

6.4. Performance Analysis of the Optimized Profile

The simulations were performed using a computational system equipped with six processing cores and hardware specifications that include 16 GB RAM, a 512 GB SSD, and an RTX 2060 6 GB graphics card. Each simulation required 40-time steps per rotor rotation and took approximately five hours to complete. With a total of 29 iterations conducted in the optimization process to achieve the highest power coefficient and solution times, the

entire simulation process spanned roughly 145 h. The use of six processing cores and the specified hardware allowed for efficient computation and facilitated the timely completion of the extensive simulations required for this study.

In this investigation, the primary goal was to optimize the power coefficient. The performance parameters, including the dimensionless power coefficient and generated power, were evaluated through 29 iterations of the optimization process to achieve the highest power coefficient and solution times. The outcomes presented in Figure 10 demonstrate that the innovative turbine design “*OR0.109BS2BN2*” attains a greater maximum power coefficient (C_p) than the reference turbine. This achievement showcases the effectiveness of the computational approach and the hardware used in the study, yielding reliable and accurate results that informed the design optimization process.

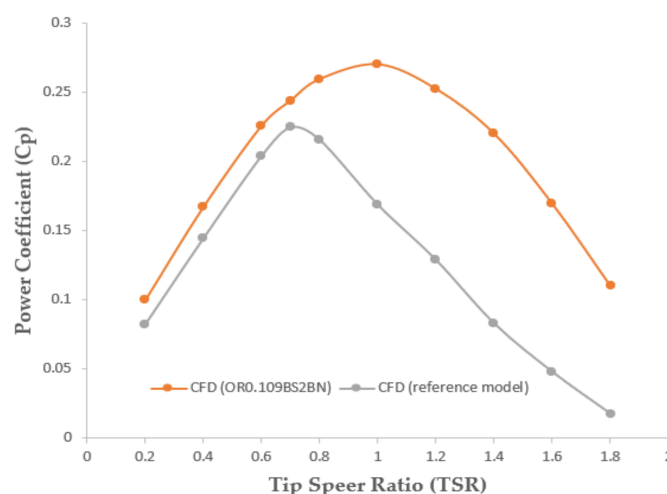


Figure 10. Comparing the reference model and the *OR0.109BS2BN2* design based on their aerodynamic performance.

The reference turbine has a maximum power coefficient ($C_p = 0.2201$) at a tip speed ratio (TSR) of 0.7. In contrast, the innovative turbine design “*OR0.109BS2BN2*” achieves a superior power coefficient ($C_p = 0.2701$) at a tip speed ratio (TSR) of 1. Compared to the reference model, the observed 22.8% enhancement in the power coefficient demonstrates that the innovative design “*OR0.109BS2BN2*” is more efficient and effective in converting wind energy into mechanical power than the reference turbine.

To further enhance performance, researchers calculated the maximum difference of optimal selection parameters between predicted and numerical results at a TSR of 1, which was found to be 2.64%. This result demonstrates the accuracy and reliability of the regression equation in predicting the performance of the Savonius wind turbine. It is essential to set the operating parameters to their optimal values to optimize the wind turbine’s performance and achieve the highest projected level. Figure 10 presents a performance comparison between the *OR0.109BS2BN2* design and the standard model. The *OR0.109BS2BN2* configuration exhibits improved performance compared to the baseline design, resulting in higher positive C_p values. However, at a specific overlap ratio, increasing the ratio raises the rotor blockage ratio for the airflow between the blades, which may lead to a lower power coefficient. Therefore, the optimal blade design represents a balance between the increased incoming air velocity and the obstruction effect created by the narrowing of the passageway due to blade tip expansion. Overall, the innovative *OR0.109BS2BN2* design demonstrates improved performance and efficiency compared to the reference turbine while maintaining a balance between essential design factors.

6.5. Flow Structure Analysis

The Reynolds number for the wind turbine in this study, calculated to be approximately 91,580, indicates that the flow regime is turbulent, which plays a significant role

in the turbine’s performance and efficiency. The turbulent flow structure analysis is crucial for understanding the complex interactions between the flow near the entrance, the rotor blades, and the local airflow dynamics. This turbulence affects the blades’ pressure distribution and aerodynamic forces, potentially leading to changes in the efficiency and power output of the turbine. Consequently, it is essential to consider these effects when designing and optimizing rotor blade profiles to maximize the wind turbine’s overall performance. The following sections will discuss the pressure distribution, blade interaction, flow velocity, and vortex formation that influence the performance of the studied wind turbine designs.

6.5.1. Pressure Distribution and Blade Interaction

Figure 11 displays the contour plots for the pressure distribution of the different geometries, revealing the highest-pressure values for the reference model and *OR0.109BS2BN2* design at a *TSR* of 1. This pressure distribution is the major source of the driving torque of the turbine at this position. In Savonius wind turbines, driving torque is generated through a drag-based mechanism due to the rotor blades’ pressure difference between the concave and convex sides. This method results in lower efficiency and rotational speeds than lift-based wind turbines such as *HAWTs* and Darrieus *VAWTs*, which rely on an aerodynamic lift to create driving torque.

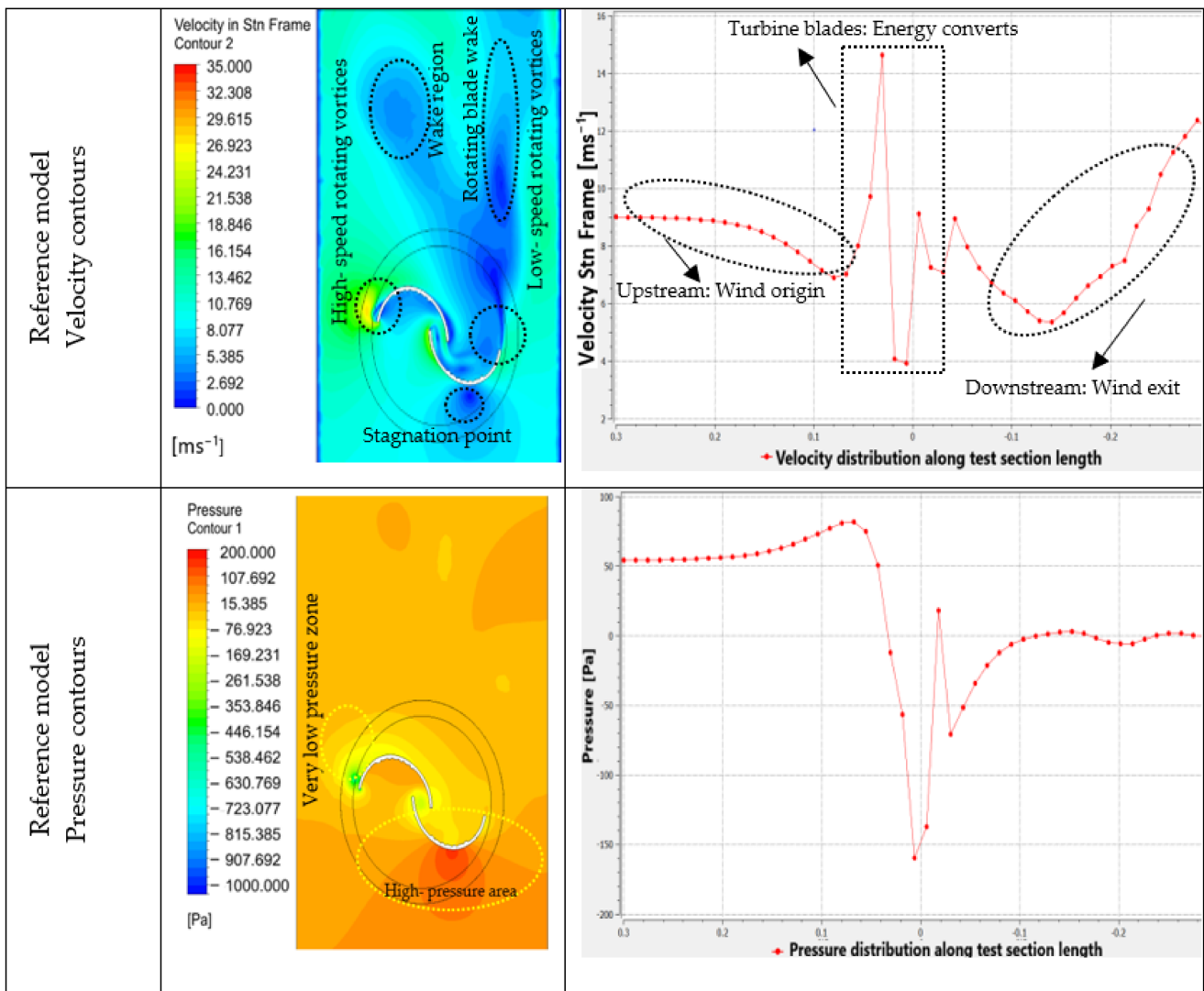


Figure 11. Cont.

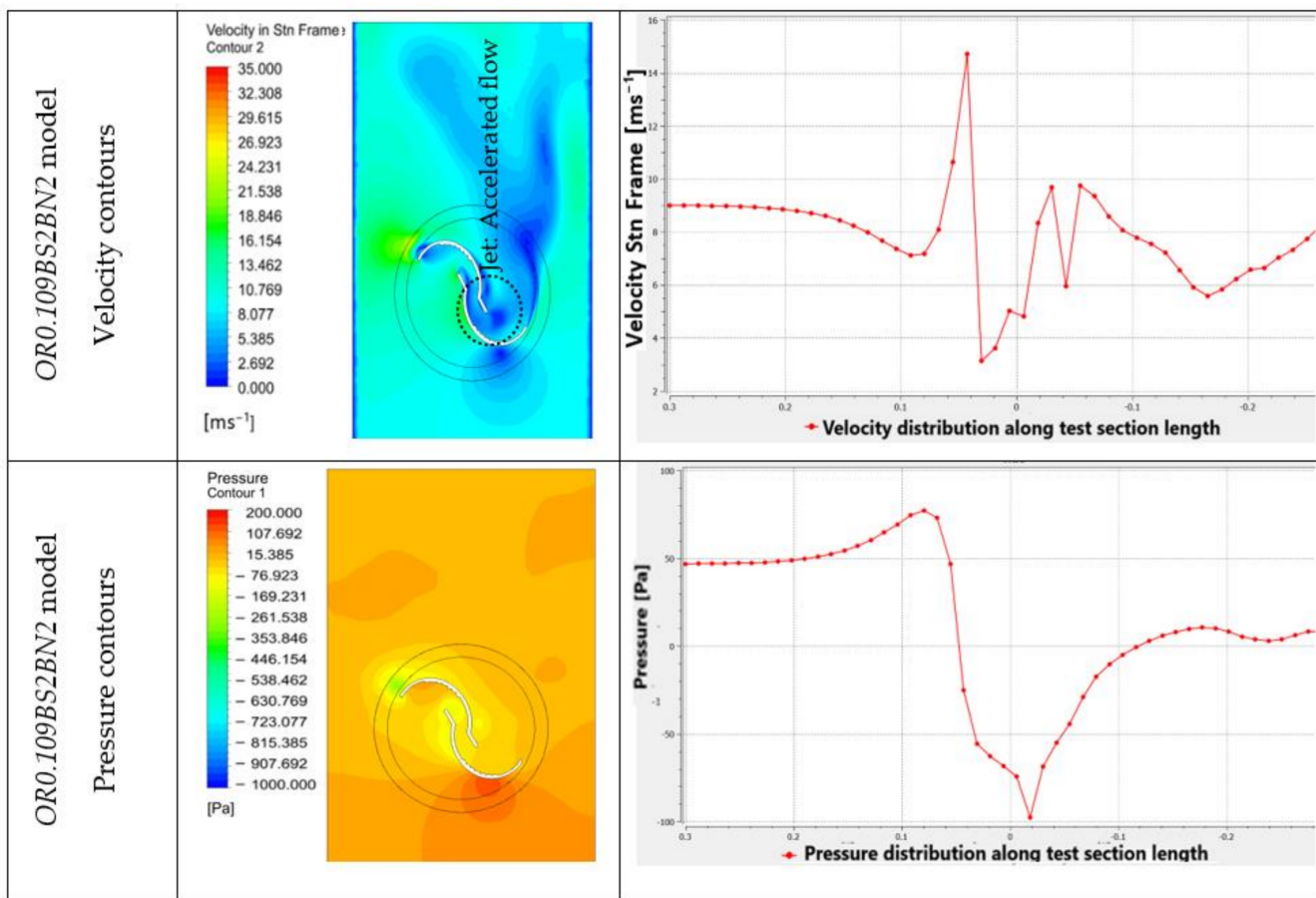


Figure 11. Velocity and pressure contours distribution along the test section.

For the reference model, the pressure distribution for the advancing blade ranged from 80 to 160 N/m², while the returning blade varied from 160 to 20 N/m². Conversely, the *OR0.109BS2BN2* design's advancing blade pressure ranged from 80 to 60 N/m², and the returning blade pressure ranged from 60 N/m² to 0. Positive pressures were noted on the inner face of the advancing blades, while negative pressures were detected near the rotation axis, on the returning blades' inner side, and the advancing blades' outer side.

In the *OR0.109BS2BN2* design, the lowest pressure values were observed at the leading edge of the advancing blades, even lower than those of the reference model. These pressure differences are responsible for driving the rotation of the Savonius wind turbine. When the *TSR* values were increased, more negative pressure values were observed on the inner side of the returning blades, near the rotation axis, and on the outer side of the advancing blades. Additionally, the *OR0.109BS2BN2* model exhibited significantly higher maximum pressure values than the reference model, indicating improved driving torque and overall performance.

6.5.2. Flow Velocity and Vortex Formation

At a *TSR* of 1, Figure 11 illustrates the velocity contours for both the reference model and the optimized model (*OR0.109BS2BN2*). Counter-rotating vortices can be observed on the inner side of the returning blades, negatively impacting the rotor's aerodynamic efficiency. The base design exhibits more vortex formation compared to the optimized design. The highest flow velocities occur at the tips of the advancing blades, where a dragging flow generates rotational torque through the lift effect, ultimately improving the wind turbine rotor's performance.

The air velocity increases on the inner side of the advancing blades, leading to a more significant negative torque on the returning blades, a phenomenon known as jet overlap.

The overlap jet is more pronounced in the optimized rotor, resulting in increased negative torque production. Furthermore, stagnation areas are present on the outer surfaces of the returning blades, reducing positive torques. At the leading edge of the advancing blade, high-velocity spinning vortices form, with wake regions developing downstream of the rotor. The reference model's advancing blade velocity ranges from 5 to 14.5 m/s, while the returning blade velocity is between 4 and 9 m/s. In contrast, the optimized model's advancing blade velocity varies from 5 to 15.25 m/s, and the returning blade velocity is between 2.5 and 7 m/s.

6.6. Flow through the Blade Gap Guide Flow

The flow within the gap between the rotor blades significantly influences torque fluctuations, with the gap vortex formation and evolution playing critical roles. The gap vortex, forming near the entrance to the gap during specific periods of the rotor's rotation, is the most crucial factor. The blade edges' geometry near the gap directly affects the vortex's magnitude and development.

Innovative blade designs aim to minimize airflow reaching the convex blades through the flow guide gap (FGG), reducing negative torque and increasing the Savonius wind turbine's power coefficient. However, modifying the blade edges' design in the gap area involves a trade-off, as it can impact other aerodynamic factors. Consequently, it is vital to carefully consider these design aspects when improving the wind turbine's performance.

Figure 12 highlights the complex flow patterns within the blade flow guide gap, specifically illustrating the areas where vortex formation and flow separation take place. The vortex formations occur in regions where the flow changes direction rapidly, causing the fluid to curl and create circular motion. Vortices can contribute to torque fluctuations in the blades and may impact the overall performance of the Savonius wind turbine.

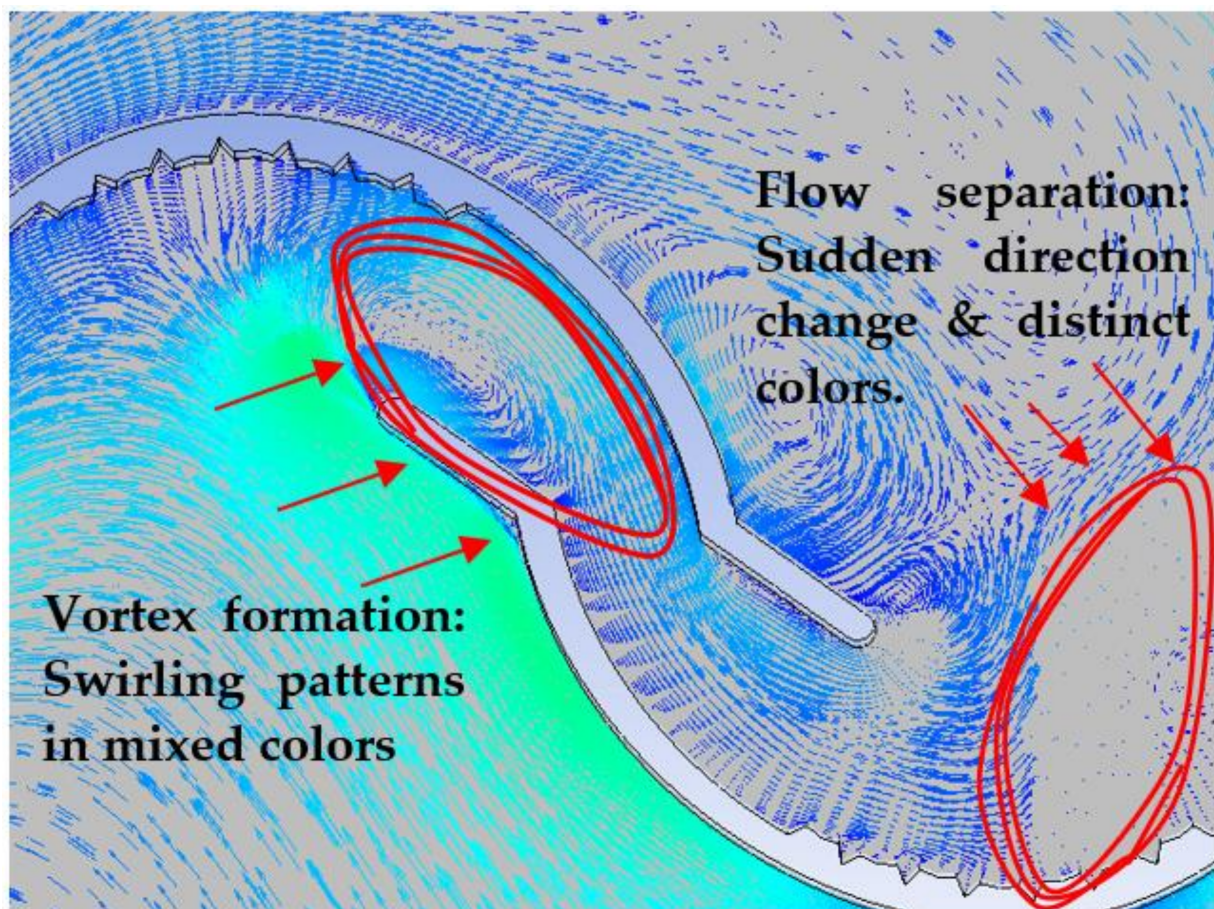


Figure 12. Velocity vectors in the blade flow guide gap.

Flow separation, on the other hand, happens when the flow detaches from the blade surface, creating an area of low pressure and recirculating flow. This phenomenon can lead to a decrease in lift and an increase in drag on the blade, ultimately affecting the turbine's efficiency.

By understanding these flow behaviors within the blade gap, researchers can identify critical aspects of the rotor design that need to be optimized to minimize the negative effects of vortex formation and flow separation. An optimized blade design may lead to improved torque generation and overall turbine efficiency.

6.7. Experimental Results

To ensure the accuracy of the numerical simulation, researchers conducted a comparison with experimental data. Due to the measuring range limitations of the torque wrench, measurements could only be performed for TSR values less than 1.6 at a flow velocity of 9 m/s.

The absence of a digital torque meter placed on the rotor shaft to measure the dynamic torque could have provided more accurate measurements of the turbine's performance. To address this limitation, incorporating a digital torque meter in future research could enhance the accuracy of the performance evaluation.

The experimental process included step-by-step stages to obtain precise measurements at different TSR values. This approach comprehensively understood the results and their correlation with the simulation data. Comparing the experimental findings with the numerical simulation led to a more reliable evaluation of the wind turbine performance.

At a flow velocity of 9 m/s, the turbine model operates at 1794 RPM, corresponding to a no-load condition. Figure 13 shows the variation of power coefficients, with the highest value found for C_p at $TSR = 0.264$. In this case, the experimental values are lower than those obtained from the numerical simulation. The discrepancy can be attributed to the fact that the 3D numerical simulation does not consider the rotor's central axis shaft in the flow field. However, these components must be addressed in the experimental setup, leading to overestimating power coefficients in the numerical simulation. Comparing and analyzing the experimental and numerical results can provide a more accurate assessment of the wind turbine's performance.

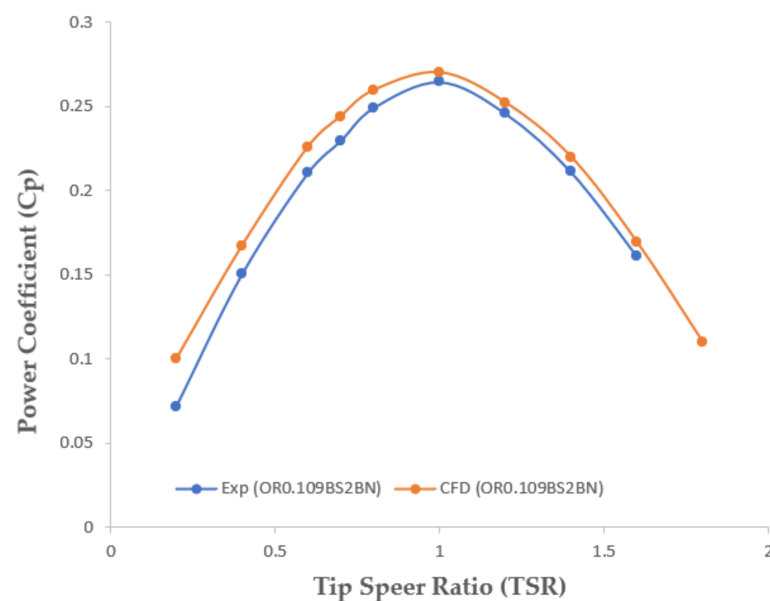


Figure 13. The power coefficient according to tip ratio speed for numerical simulations and experiments.

The power coefficient variation increases, starting at 0.07 for a tip speed ratio (TSR) of 0.2 and peaking at 0.264 when $TSR = 1$. The average deviation of C_p across TSR ranges

[0.2 to 1] and [1 to 1.6] is about 7%. Notably, the numerical curve closely aligns with actual data within the [1 to 1.6] *TSR* range, yielding accurate predictions with minimal errors.

7. Conclusions

In summary, this study effectively employed *ANSYS CFX* simulations and a robust experimental approach, successfully validating the utilized methods. These results lend confidence to the accuracy and reliability of the findings presented in this report. The research also conducted an in-depth examination of a novel Savonius turbine blade, evaluating the effects of overlap ratio, blade profile, and blade number on the performance of Savonius turbines. The literature would benefit from more research addressing the influence of inner blade configuration.

Moreover, the study explored the Design of Experiments (*DOE*) approach to enhance the aerodynamic properties of wind turbines, leading to the establishment of three key parameters, each with two distinct levels. A wind tunnel experiment was conducted to validate the data-driven findings and primary analysis, providing valuable insights and contributing to the overall understanding of Savonius turbine optimization.

- The research successfully identified the optimal blade configuration for the new inner blade profiles from ten models, selecting the one that generates the most power. The addition of flow guide gaps to the ten models resulted in improved Savonius wind turbine performance.
- Researchers investigated three different parameters, each with two levels, to improve the aerodynamic performance of a Savonius wind turbine. After conducting eight numerical analyses for $TSR = 1$, they determined that the *OR0.109BS2BN2* model (elliptical blade profile with inner wavy area, overlap ratio of 0.109, and two blades) had the highest power coefficient and was the optimal rotor for maximizing C_p .
- Various criteria were prioritized based on relative importance, with the overlap ratio as the most critical factor. The mathematical model established the relationships between the three parameters and the power coefficient, with R^2 errors having the minimum values. *ANOVA* studies were conducted to determine the impact of certain factors. For the *OR0.109BS2BN2* design, *CFD* simulations were performed between 0.2 and 1.8 *TSR*.
- Increasing the overlap distance reduces the efficiency because the returning flow becomes turbulent, hindering the directed flow from fully connecting with the forward blade, thus decreasing the efficiency to some extent. Further research and investigation into the gap guide's flow angle fluctuation are necessary to achieve optimal conditions.
- With the optimal arrangement in the inner wavy place, the aerodynamic performance of the Savonius rotor was enhanced at all *TSR* values. At higher *TSR* values, the aerodynamic performance gap between the basic and *OR0.109BS2BN2* design was projected to be larger. The optimized design increased the observed C_p by 22.8% when the *TSR* was equal to one.
- A trade-off was observed between the flow (swirling flow) through the gap guide flow and the impact blockage ratio, which resulted from the reduced channel width caused by the extended blade tip length. These trade-offs should be carefully considered when optimizing the design, as they may impact the wind energy conversion system's overall aerodynamic performance, efficiency, and power output.

Future research could focus on developing hybrid wind turbine systems, combining the optimized Savonius rotor with other designs, such as horizontal-axis or Darrieus turbines. These hybrid configurations' complementary characteristics may enhance efficiency and power output in variable wind conditions.

Author Contributions: Conceptualization, K.A.H.A.-G. and F.B.I.A.; methodology, K.A.H.A.-G. and B.A.J.A.-q.; software, A.K.K.; validation, F.B.I.A., B.A.J.A.-q. and E.S.T.; data curation, K.A.H.A.-G. and A.K.K.; writing—original draft preparation, K.A.H.A.-G.; writing—review and editing, K.A.H.A.-G., F.B.I.A. and B.A.J.A.-q.; supervision, F.B.I.A., B.A.J.A.-q. and E.S.T. All authors have read and agreed to the published version of the manuscript.

Funding: This research received no external funding.

Institutional Review Board Statement: Not applicable.

Informed Consent Statement: Not applicable.

Data Availability Statement: The data presented in this study are available on request from the corresponding author.

Conflicts of Interest: The authors declare no conflict of interest.

References

- Satwika, N.A.; Hantoro, R.; Sarwono, S.; Nugroho, G. Experimental investigation and numerical analysis on horizontal axis wind turbine with winglet and pitch variations. *Eng. J.* **2019**, *23*, 345–360. [\[CrossRef\]](#)
- Tahani, M.; Rabbani, A.; Kasaeian, A.; Mehrpooya, M.; Mirhosseini, M. Design and numerical investigation of Savonius wind turbine with discharge flow directing capability. *Energy* **2017**, *130*, 327–338. [\[CrossRef\]](#)
- Chang, T.L.; Tsai, S.F.; Chen, C.L. Optimal design of novel blade profile for savonius wind turbines. *Energies* **2021**, *14*, 3484. [\[CrossRef\]](#)
- Alom, N.; Saha, U.K. Drag and lift characteristics of a novel elliptical-bladed savonius rotor with vent augmenters. *J. Sol. Energy Eng. Trans. ASME* **2019**, *141*, 051007. [\[CrossRef\]](#)
- Gerrie, C.; Islam, S.Z.; Gerrie, S.; Turner, N.; Asim, T. 3D CFD Modelling of Performance of a Vertical Axis Turbine. *Energies* **2023**, *16*, 1144. [\[CrossRef\]](#)
- Alom, N. Influence of curtain plates on the aerodynamic performance of an elliptical bladed Savonius rotor (S-rotor). *Energy Syst.* **2021**, *13*, 265–280. [\[CrossRef\]](#)
- Roy, S.; Saha, U.K. Review of experimental investigations into the design, performance and optimization of the Savonius rotor. *Proc. Inst. Mech. Eng. Part A J. Power Energy* **2013**, *227*, 528–542. [\[CrossRef\]](#)
- Vicente, J.; Antonio, H.; Prisco, A. A review on the performance of Savonius wind turbines. *Renew. Sustain. Energy Rev.* **2012**, *16*, 3054–3064. [\[CrossRef\]](#)
- Dorel, S.F.; Mihai, G.A.; Nicusor, D. Review of Specific Performance Parameters of Vertical Wind Turbine Rotors Based on the SAVONIUS Type. *Energies* **2021**, *14*, 1962. [\[CrossRef\]](#)
- Alom, N.; Saha, U.K. Evolution and progress in the development of savonius wind turbine rotor blade profiles and shapes. *J. Sol. Energy Eng. Trans. ASME* **2019**, *141*, 030801. [\[CrossRef\]](#)
- Bhutta, M.M.A.; Hayat, N.; Farooq, A.U.; Ali, Z.; Jamil, S.R.; Hussain, Z. Vertical axis wind turbine—A review of various configurations and design techniques. *Renew. Sustain. Energy Rev.* **2012**, *16*, 1926–1939. [\[CrossRef\]](#)
- Al-Faruk, A.; Sharifian, A. Geometrical optimization of a swirling Savonius wind turbine using an open jet wind tunnel. *Alex. Eng. J.* **2016**, *55*, 2055–2064. [\[CrossRef\]](#)
- Alit, I.; Andyani, I.S.; Mirmanto, M. Effect of Overlapping Ratio, Blade Shape Factor, and Blade Arc Angle to modified Rotor Savonius performances. *Int. J. Appl. Eng. Res.* **2018**, *13*, 411–416.
- Ebrahimpour, M.; Shafaghat, R.; Alamian, R.; Shadloo, M.S. Numerical investigation of the Savonius vertical axis wind turbine and evaluation of the effect of the overlap parameter in both horizontal and vertical directions on its performance. *Symmetry* **2019**, *11*, 821. [\[CrossRef\]](#)
- Alom, N.; Saha, U.K. Arriving at the optimum overlap ratio for an elliptical-bladed savonius rotor. *Proc. ASME Turbo Expo* **2017**, *9*, 1–10. [\[CrossRef\]](#)
- Hassanzadeh, R.; Mohammadnejad, M. Effects of inward and outward overlap ratios on the two-blade Savonius type of vertical axis wind turbine performance. *Int. J. Green Energy* **2019**, *16*, 1485–1496. [\[CrossRef\]](#)
- Lajnef, M.; Mosbahi, M.; Chouaibi, Y.; Driss, Z. Performance Improvement in a Helical Savonius Wind Rotor. *Arab. J. Sci. Eng.* **2020**, *45*, 9305–9323. [\[CrossRef\]](#)
- Im, H.; Kim, B. Power Performance Analysis Based on Savonius Wind Turbine Blade Design and Layout Optimization through Rotor Wake Flow Analysis. *Energies* **2022**, *15*, 9500. [\[CrossRef\]](#)
- Ostos, I.; Ruiz, I.; Gajic, M.; Gómez, W.; Bonilla, A.; Collazos, C. A modified novel blade configuration proposal for a more efficient VAWT using CFD tools. *Energy Convers. Manag.* **2019**, *180*, 733–746. [\[CrossRef\]](#)
- Torres, S.; Marulanda, A.; Montoya, M.F.; Hernandez, C. Geometric design optimization of a Savonius wind turbine. *Energy Convers. Manag.* **2022**, *262*, 115679. [\[CrossRef\]](#)
- Gallo, L.A.; Chica, E.L.; Flórez, E.G. Numerical Optimization of the Blade Profile of a Savonius Type Rotor Using the Response Surface Methodology. *Sustainability* **2022**, *14*, 5596. [\[CrossRef\]](#)

22. Al Absi, S.M.; Jabbar, A.H.; Mezan, S.O.; Al-Rawi, B.A.; Alattabi, S.T. An experimental test of the performance enhancement of a Savonius turbine by modifying the inner surface of a blade. *Mater. Today Proc.* **2021**, *42*, 2233–2240. [[CrossRef](#)]
23. Shahizare, B.; Nik-Ghazali, N.; Chong, W.T.; Tabatabaeikia, S.; Izadyar, N.; Esmailzadeh, A. Novel investigation of the different Omni-direction-guide-vane angles effects on the urban vertical axis wind turbine output power via three-dimensional numerical simulation. *Energy Convers. Manag.* **2016**, *117*, 206–217. [[CrossRef](#)]
24. Hamzah, I.; Prasetyo, A.; Tjahjana, D.P.; Hadi, S. Effect of blades number to performance of Savonius water turbine in water pipe. *AIP Conf. Proc.* **2018**, *1931*, 030046. [[CrossRef](#)]
25. Wenehenubun, F.; Saputra, A.; Sutanto, H. An experimental study on the performance of Savonius wind turbines related with the number of blades. *Energy Procedia* **2015**, *68*, 297–304. [[CrossRef](#)]
26. Ali, M.H. Experimental Comparison Study for Savonius Wind Turbine of Two & Three Blades at Low Wind Speed. *Int. J. Mod. Eng. Res.* **2013**, *3*, 2978–2986.
27. Al-Gburi, K.A.H.; Al-quraishi, B.A.J.; Alnaimi, F.B.I.; Tan, E.S.; Al-Safi, A.H.S. Experimental and Simulation Investigation of Performance of Scaled Model for a Rotor of a Savonius Wind Turbine. *Energies* **2022**, *15*, 8808. [[CrossRef](#)]
28. Tian, W.; Ni, X.; Mao, Z.; Wang, Y.F. Study on the performance of a new VAWT with overlapped side-by-side Savonius rotors. *Energy Convers. Manag.* **2022**, *264*, 115746. [[CrossRef](#)]
29. Shkhair, M.M.; Jaber, O.K.; Al Absi, S.M. Effect of Rotor Blades Number and Rotor Position on the Performance of a Diffuser Augmented Wind Turbine. *Int. J. Mech. Eng. Robot. Res.* **2022**, *11*, 858–864. [[CrossRef](#)]
30. Lee, J.H.; Lee, Y.T.; Lim, H.C. Effect of twist angle on the performance of Savonius wind turbine. *Renew. Energy* **2016**, *89*, 231–244. [[CrossRef](#)]
31. D’Alessandro, V.; Montelpare, S.; Ricci, R.; Secchiaroli, A. Unsteady Aerodynamics of a Savonius wind rotor: A new computational approach for the simulation of energy performance. *Energy* **2010**, *35*, 3349–3363. [[CrossRef](#)]
32. Nasef, M.H.; El-Askary, W.A.; AbdEL-hamid, A.A.; Gad, H.E. Evaluation of Savonius rotor performance: Static and dynamic studies. *J. Wind Eng. Ind. Aerodyn.* **2013**, *123*, 1–11. [[CrossRef](#)]
33. Damak, A.; Driss, Z.; Abid, M.S. Optimization of the helical Savonius rotor through wind tunnel experiments. *J. Wind Eng. Ind. Aerodyn.* **2018**, *174*, 80–93. [[CrossRef](#)]
34. Talukdar, P.K.; Sardar, A.; Kulkarni, V.; Saha, U.K. Parametric analysis of model Savonius hydrokinetic turbines through experimental and computational investigations. *Energy Convers. Manag.* **2018**, *158*, 36–49. [[CrossRef](#)]
35. Moffat, R.J. Describing the uncertainties in experimental results. *Exp. Therm. Fluid Sci.* **1988**, *1*, 3–17. [[CrossRef](#)]
36. Kaya, A.F.; Acir, A. Enhancing the aerodynamic performance of a Savonius wind turbine using Taguchi optimization method. *Energy Sources Part A Recover. Util. Environ. Eff.* **2022**, *44*, 5610–5626. [[CrossRef](#)]
37. Sheikh, H.M.; Shabbir, Z.; Ahmed, H.; Waseem, M.H.; Sheikh, M.Z. Computational fluid dynamics analysis of a modified Savonius rotor and optimization using response surface methodology. *Wind Eng.* **2017**, *41*, 285–296. [[CrossRef](#)]

Disclaimer/Publisher’s Note: The statements, opinions and data contained in all publications are solely those of the individual author(s) and contributor(s) and not of MDPI and/or the editor(s). MDPI and/or the editor(s) disclaim responsibility for any injury to people or property resulting from any ideas, methods, instructions or products referred to in the content.